1. **Title**

The effect of convective motion within liquid fuel on the mass burning rates of pool fires – a numerical study

2. **Authors**

Baopeng Xu, Jennifer Wen

3. **Corresponding author's COMPLETE contact information:**

Jennifer Wen (Dr.)
School of Engineering
University of Warwick
Coventry CV4 7AL, UK
Phone: +44 (0)24 765 73365
Email. Jennifer.wen@warwick.ac.uk

4. **Colloquium that describes the research topic**

Fire research

5. **Total length of paper and method of determination**

Method 1

6188 words

6. **List word equivalent lengths for main text, nomenclature, references, each figure with caption, and each table determined according to the instructions that follow**

Text: 3237 words

References: 507 words

Figures total: 1889 words

Figure 1: 133 words; Figure 2: 211 words; Figure 3: 484 words; Figure 4: 244 words; Figure 5: 282 words; Figure 6: 238 words; Figure 7:163 words; Figure 8: 163 words;

Equations: 281 words;

Table 1: 76 words.

Table 2: 198 words.

Abstract

To improve numerical simulation of liquid pool fires and remove the need for experimentally measured or empirically calculated mass burning rates as boundary conditions, a fully coupled three-dimensional (3-D) numerical formulation, which directly solves convective motion in the fuel region by incorporating inhomogeneous heat feedback, is formulated. The fire dynamics is modelled using the large eddy simulation (LES) approach. Incompressible laminar flow formation is applied to the liquid fuel region, assuming constant thermo-physical properties except for the density which follows the Boussinesq approximation. The numerical formulation of the two phases is solved using a fully coupled conjugate heat transfer approach at the pool surface. The coupled model is validated against published measurements for a thin-layer heptane pool fire and a deep methanol pool fire. The convective motion within the liquid phase is found to have important effects on the pool fire mass burning rate and its neglection would result in a fast rise and over-prediction of the mass burning rate.

Keywords

Pool fire; mass burning rate; Marangoni effect; conjugate heat transfer; large eddy simulation

1. Introduction

Liquid pool fires are often present in accidental fire scenarios in the process industry resulting from fuel spills and storage tanks. The combustion of pool fires is self-driven by the closely coupled heat and mass transfer between the flame and the liquid fuel. The heat feedback from the flame to the liquid fuel determines the burning rate of pool fires, which sustains the flame.

Previous experimental studies have included both thin-layer [1-4] and deep pool fires [5-8]. Their burning behaviour differs in two aspects. Firstly, the fuel level of the thin-layer pools regresses with the progress of the combustion; while that of the deep pools remains almost constant with continuous fresh fuel being added through the pool bottom [6]. Secondly, the burning process of thin-layer pool fires is highly transient [9] while deep pool fires can reach a quasi-steady state after a warm-up period [6]. Many factors can affect the burning rate, for instance the fuel type, size and depth of the liquid pool, material and geometry of the fuel container as well as ambient conditions, etc. Because of these complicated influencing factors, the measured burning rates often differ even for the same pool size and fuel type during experimental investigations [10].

The heat feedback from the flame to the pool surface is in the forms of radiation and convection, while conduction mainly contributes to the heat transfer at the container walls. The role of radiation becomes more important for sootier fuels and larger pool sizes. It was found that heat conduction via the container walls is only important for very small pool fires [11]. Liquid fuels are not usually considered to be optically thin, and the in-depth radiation into the fuel region is normally absorbed within several millimetres [2]. As the heat feedback enters the fuel, it is redistributed via conduction, convection and in-depth radiation [12].

The puffing nature of pool fires creates unsteady inhomogeneous heat feedback, resulting in transient non-uniform distribution of the mass burning rate. It was found that the burning rate can be higher at the centre [13] or at the outer ring [14], depending on the experimental conditions. The inhomogeneous heat feedback also creates significant surface temperature gradient, which would lead to hydrodynamic instability through Marangoni effect [15], which induces vortex motions inside the fuel, enhancing its heat transfer coefficient.

The development of a physics-based fully coupled numerical model to predict the burning rate needs to consider a large number of coupled parameters associated with both the gas phase and liquid flows. Most previous numerical studies avoided the solution of the liquid phase by directly applying a prescribed fuel mass flow rate from experimental measurement [16] or simplified empirical correlations [17] at the fuel inlet boundary. To truly capture the underlying physics, the liquid phase needs to be solved along with the gas phase solver. The most popular evaporation model to predict the burning rate in the literature is based on the 'film theory' where evaporation is driven by a diffusion process and liquid-vapour equilibrium is assumed at the pool surface temperature [18, 19]. The 'film theory' based model is capable of capturing the transient nature of the burning processes by allowing for the evaporation below the boiling point.

However, most previous numerical studies on the burning rate neglected the convective motion in the liquid phase. An alternative approach to adjust the thermal conductivity to consider the internal convection was attempted by using the convective heat transfer coefficient [18]. A faster rise of the initial burning rate was generally predicted in these numerical studies. This is due to the neglect of the convective motion which tends to enhance the heat transfer in the liquid fuel. Very recently, Fukumoto et al. [20] numerically investigated the vortex motions of a steady small-scale methanol

pool fire, using fully compressible description for the liquid pool. Their study revealed that the Marangoni effect and the heat transfer from the sidewall had little influence on the steady burning rate; but neglecting buoyancy effect in the liquid phase surprisingly resulted in almost 64% reduction in the steady mass burning rate.

The convective motion in the liquid phase is induced by both the Marangoni and buoyancy effects. The Marangoni effect, resulting from the surface temperature gradient, is more pronounced at the heat-up stage, is expected to play a more important role for the transient burning rate. In the present study, a fully coupled 3-D numerical formulation is formulated to explicitly solve the convective motion in the liquid fuel. The numerical formulation is validated against both thin-layer pool fire and deep pool fire tests. In-depth analysis is performed to investigate the effects of liquid flow motions on the transient burning rates and inhomogeneous distributions of field variables on the pool surface.

2. Numerical formulation

The aim of this study is to formulate a fully coupled 3-D model considering the convective motion in the liquid phase by incorporating both the Marangoni and buoyancy effects. The computational domain is partitioned into a fire region and a fuel region for which different governing equations are formulated to describe the underlying physics.

2.1 Fire region

The turbulent pool fire is simulated by the in-house version of FireFOAM [21], the LES based fire simulation solver within open source CFD code, OpenFOAM. The fire dynamics is described by a set of filtered compressible Navier-Stokes equations including the buoyancy effect. The equations

are closed by a one-equation sub-grid scale (SGS) turbulence model [22]. The turbulent combustion is assumed to be mixing-controlled and modelled by the Eddy Dissipation Concept (EDC) which was modified and extended into the LES framework by Chen et al. [16]. Soot volume fraction is modelled by the laminar smoke point-based soot model for turbulent fires also developed by Chen et al. [16]. The soot model was validated against a 0.3 m heptane pool fire, and the predicted and measured mean temperature and soot volume fraction were found to be in relatively good agreement with the measurements [16]. The transport equations for the radiative heat transfer are solved by the finite volume based discrete ordinate method [16]. More information about FireFOAM and the sub-models used can be found in [16, 21].

2.2 Fuel region

The fuel region exchanges mass and heat with the fire region at the phase interface. The convective motion in the fuel region is in small scales and tends to gradually attenuate during the heat-up process. Therefore, incompressible laminar transport is formulated by assuming constant thermo-physical properties except for the density which follows the Boussinesq approximation.

$$\nabla \cdot \boldsymbol{u} = 0 \tag{1}$$

$$\frac{\partial \boldsymbol{u}}{\partial t} + \nabla \cdot (\boldsymbol{u}\boldsymbol{u}) = -\nabla p + \mu \nabla^2 \boldsymbol{u} + \left[1 - \beta_l \left(T - T_{ref}\right)\right]\boldsymbol{g} \tag{2}$$

$$\frac{\partial T}{\partial t} + \nabla \cdot (\boldsymbol{u}T) = \alpha \nabla^2 T + \frac{\partial Q_{dep}}{\partial \boldsymbol{n}} \frac{1}{\rho C_p} \tag{3}$$

Where $\boldsymbol{u}$ is the velocity vector, t the time, p the pressure, μ the viscosity, β_l the coefficient of thermal expansion, T the temperature, T_{ref} the reference temperature, $\boldsymbol{g}$ the gravitational force, $\alpha = {}^{k}/_{\rho C_p}$ the thermal diffusivity, and k is the thermal conductivity, ρ the density, C_p the specific heat at constant pressure, Q_{dep} the source term of in-depth radiation, $\boldsymbol{n}$ the normal vector of pool

surface.

Q_{dep} is calculated according to the Beer's law [23]:

$$Q_{dep} = Q_r exp(-\alpha \cdot \Delta_{dep}) \quad (4)$$

where Q_r is the net radiative heat flux at the pool surface, α the fuel absorption coefficient, Δ_{dep} is the distance from the pool surface.

2.3 Evaporation model

The evaporation model used in this study follows the widely used 'film theory' model proposed by Sikanen and Hostikka [18], which is based on the liquid-vapour equilibrium assumption. It assumes an existence of a fuel vapour diffusion layer, not suitable for the boiling burning stage. For more information on the model please refer to the reference [18].

2.4 Boundary conditions

The numerical formulas for the fire and fuel regions need to be closed by the interface boundary conditions governing the continuity of mass, energy and momentum at the interfaces.

2.4.1 Thermal boundary condition

At the pool surface the following equations applies:

$$T_{f,int} = T_{g,int} \quad (5)$$

$$k_f \frac{\partial T_f}{\partial n}\Big|_{int} + \dot{m}''\Delta H_v = k_g \frac{\partial T_g}{\partial n}\Big|_{int} \quad (6)$$

where subscripts f, g and int denote fuel, gas and phase interphase, respectively. k_f is the fuel thermal conductivity and k_g is the gas mixture-averaged thermal conductivity.

The first term on the left side of Eq. (6) is the convective heat transfer. Since the Reynolds number is rather small at the pool surface and there is also a mass flux at the surface, it is decided to resolve the flow adjacent to the surface.

2.4.2 Velocity boundary conditions

The Marangoni convection velocity at the fuel surface is related to the surface tension gradient by neglecting the shear contributions from the gas phase:

$$\mu \frac{\partial u}{\partial z} = \frac{\partial \sigma}{\partial T} \frac{\partial T}{\partial x} \tag{7}$$

$$\mu \frac{\partial v}{\partial z} = \frac{\partial \sigma}{\partial T} \frac{\partial T}{\partial y} \tag{8}$$

where u and v are the velocity components at the pool surface, and $\frac{\partial \sigma}{\partial T}$ is the temperature coefficient of surface tension. To prevent the deformation of the pool surface, the vertical component is calculated by:

$$w = \frac{\sum \dot{m}_i'' A_i}{\rho_f \sum A_i} \tag{9}$$

where $\dot{m}_i''$ is the mass burning rate, A_i the area of cell faces at the pool surface. The vertical velocity is used for updating both the liquid phase mesh and the gas phase mesh within the container by uniformly redistributing the mesh points in the vertical direction for the transient thin-layer pool fire.

The inlet velocity of the gas phase is calculated by:

$$\boldsymbol{u}_i^g = \frac{\dot{m}_i''}{\rho_g A_i} \cdot \boldsymbol{n} + \boldsymbol{u}_i^f \tag{10}$$

where $\boldsymbol{u}_i^g$ and $\boldsymbol{u}_i^f$ are the velocity vectors of the gas phase and the liquid phase at the interface.

Table 1 Test conditions.

Test	Burner Diameter (m)	Burner depth (m)	Initial fuel depth (m)	Fuel temperature (K)
Heptane	0.3	0.04	0.013	284.5
Methanol	0.3	0.15	0.145	295.0

3. Problem descriptions

The proposed model was validated against a thin-layer heptane pool fire [1] and a deep methanol pool fire [7]. The former produces a sooty flame while the methanol fire is soot free. Both fire tests used a 0.3 m diameter circular burner. The test conditions are listed in Table 1 and the fuel properties in Table 2. Constant fuel properties were assumed, and their variations were found to be less than 15% within the range of the considered temperature.

Table 2 Liquid fuel properties.

Properties	Values	
	Heptane	Methanol
Density kg/m^3	675	794
Specific Heat $kJ/(kg \cdot K)$	2.24	2.48
Thermal Conductivity $W/(m \cdot K)$	0.14	0.20
Heat of Vaporization kJ/kg	317	1088
Viscosity m^2/s	5.5×10^{-7}	13.9×10^{-7}
Coefficient of Thermal Expansion $1/K$	1.24×10^{-3}	1.18×10^{-3}
Boiling Point K	371.5	337.7
Absorption Coefficient m^{-1}	493[26]	1140[27]
Temperature Coefficient of Surface Tension $mN/(m \cdot K)$	-0.098	-0.077

The cylindrical computational domain for both the heptane and methanol pool fires has a diameter of 1.65 m and a height of 2.5 m. The fuel container is centrally located at the bottom plane of the computational domain. The fire region mesh is refined above the pool surface in the vertical direction. The pool surface is discretized into around 1500 cells for both cases. The mesh size for the

fire region is approximately 320,000 for both cases, and the mesh size for the fuel region is roughly 60,000 for the thin-layer case and 180,000 for the deep pool case. To resolve the gas flow at the pool surface, the meshes inside the burner lips are refined with a 1 mm cell size in the vertical direction, which corresponds to $Y^+ < 1.5$. Our preliminary grid sensitivity study has confirmed that the adopted grid resolutions were sufficient and further refinement of the grid resolution did not improve the predictions.

For the extended EDC combustion model, a single step global chemical mechanism is used with 5 species included in the simulations. For the soot model, the laminar smoke point height is set to 0.147m for heptane following [16]. The radiative properties of both gas and liquid phase are treated as gray. A total of 16 solid angles covering the hemisphere are used for the radiative transfer equations as a compromise between computational time and accuracy.

To initiate the evaporation process, the simulations started from an initial burning rate of 0.003 $kg/(m^2 \cdot s)$ which was found to be the lowest initial rate to achieve a quick ignition. For the 0.3 m pool fires, in order to accurately predict the heat conduction, the fuel container needs to be included as an additional computational region, which would make the solution more complicated with limited benefit. Therefore, the heat conduction is neglected by setting an adiabatic boundary condition at the container walls. It needs to be pointed out that this treatment can incur errors for the thin-layer pool fire as the heat loss through the bottom wall affects the burning rate [1]. The lateral and the top boundaries of the fire region were set as a free boundary condition. Finally, a moving boundary was set for the pool surface to allow for the surface regression for the transient thin-layer case, while the pool surface was fixed for the steady deep pool fire during the simulations.

Fig. 1. Comparison between the predicted flame shapes (bottom) with the images from the methanol fire test [7].

4. Results and discussion

4.1 The steady methanol pool fire

Figure 1 compares two images of the pulsating methanol pool fire. The two images on the top are reproduced from reference [7], and the images at the bottom are from the current simulation plotted with the iso-surface of T=700 K. The anchored necking flame is well captured by the predictions. The predicted puffing frequency is 2.65 Hz, close to the experimental data of 2.8 Hz.

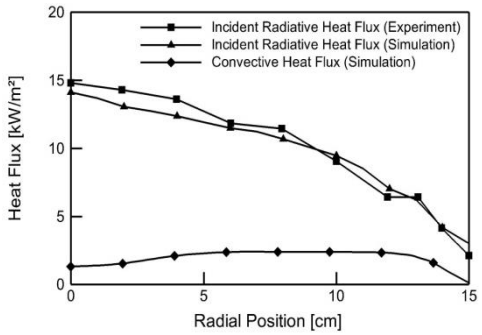

Fig. 2. The time-averaged convective and incident radiative heat fluxes at the pool surface for the methanol fire.

The time-averaged incident radiative heat flux distribution for the methanol fire is displayed and compared to measurement favourably in Fig. 2. The averaged flux is high in the centre and gradually decreases toward the rim. The predicted convective heat flux is also plotted in Fig. 2. The convective heat flux is much smaller than the radiative heat flux due to the relatively small flow velocity at the pool surface.

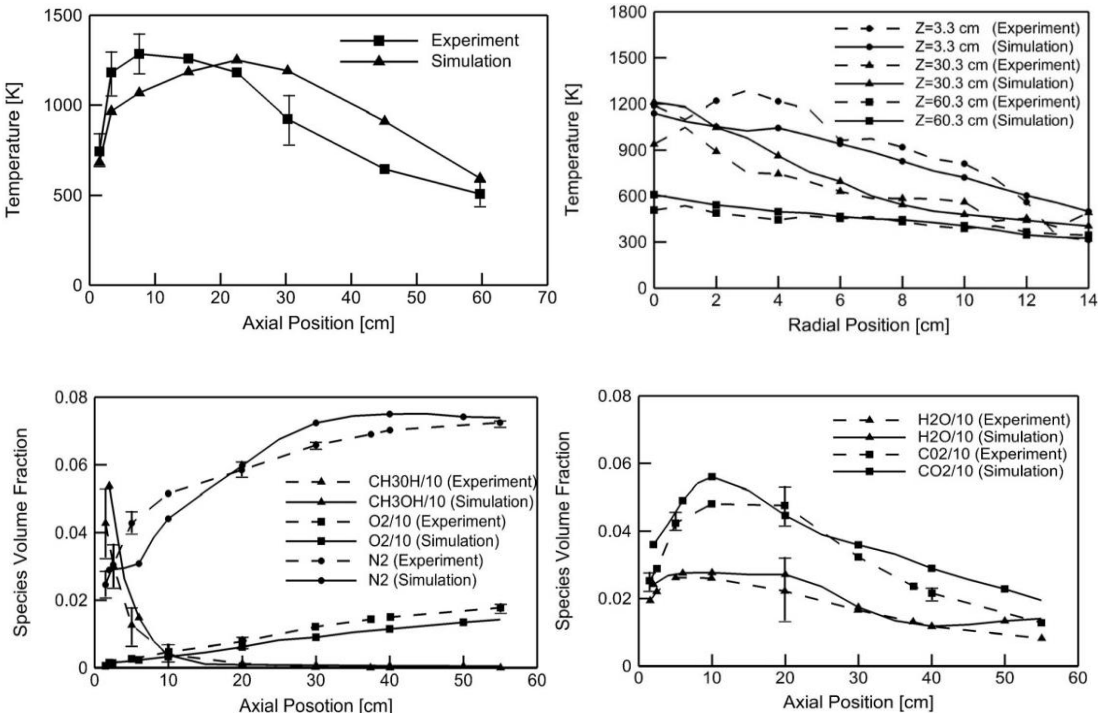

Fig. 3. Comparison between the predicted and measured gas phase time-averaged temperatures and species concentrations for the methanol fire.

Comparison between the predicted and measured time-averaged temperatures and species concentrations along the centreline are displayed in Fig. 3 for the methanol fire, demonstrating reasonably good agreement in the values, but the location of the predicted maximum temperature is higher than the measured one. The predicted temperature profiles at three vertical locations above the

burner are also in line with the measured profiles but relatively large discrepancies exist near the pool surface which falls in the persistent flame region. The predicted species concentrations along the centreline are also in reasonably good agreement with the measurements.

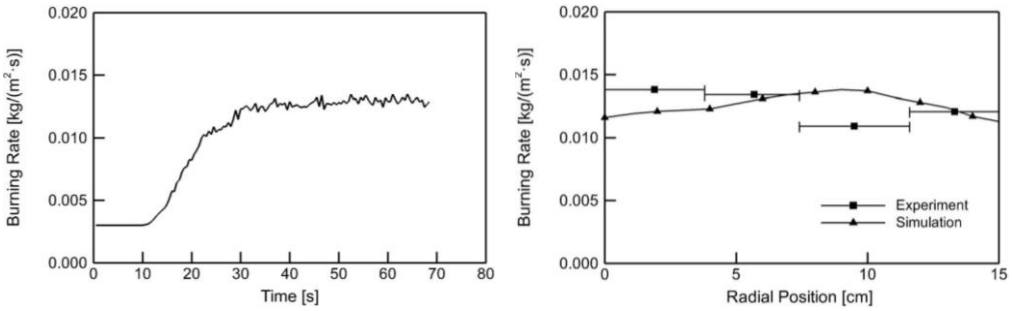

Fig. 4. The predicted mass burning rate *vs* time and comparison between the predicted and measured [7] time-averaged distribution at the pool surface.

Figure 4 shows the predicted mass burning rate *vs* time. The burning rate remains unchanged prior to 12 s during the numerical ignition process due to the relatively low radiative heat feedback, and then increase quickly to a quasi-steady value of 0.013 $kg/(m^2 \cdot s)$ at 30 s. The burning rate on the right-hand plot in Fig. 4 is the time-averaged value for the quasi-steady state. The measurements were from reference [6] where the burner of the same size was divided into 4 annular rings to measure the burning rate distribution along the radial direction. Overall, the predicted distribution is in good agreement with the measured profile. The measured burning rate was high at the centre and the lowest value was observed at r = 10 cm, while the maximum burning rate was predicted around r = 10 cm. Some discrepancies exist elsewhere and might be caused by the simplification of the boundary conditions and experimental uncertainties. Moreover, as the test burner was divided into 4 unconnected annular rings which prohibited the surface flow motions, this might also incur some deviation from the actual physics.

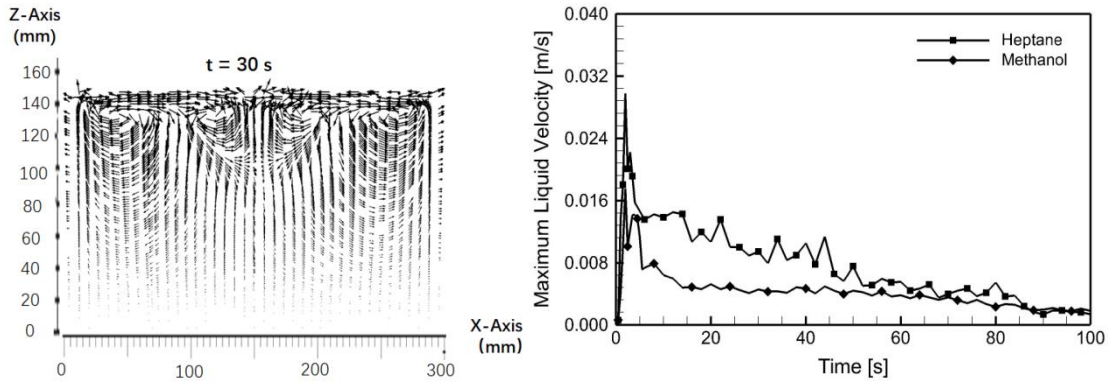

Fig. 5. The predicted velocity vectors at the middle plane for the methanol fire and the maximum velocity in the fuel region.

Figure 5 shows the predicted velocity vectors at the middle plane for the methanol fire and the maximum velocity in the fuel region. The former reveals clear vortex motion. The convective motion is more pronounced at the top and the velocities are much lower near the bottom. Four counter-rotating vortices are predicted at 30 s. The counter-rotating vortices were also experimentally observed in Vali's methanol pool fire tests [25]. The predicted number and locations of the vortices vary with time. The convective motion is more pronounced during the heat-up stage, as evident by the maximum flow velocity also plotted in Fig. 5. The convective motion is more significant for the heptane fire than the methanol fire due to the relatively larger radiative heat feedback. For both fires, the maximum velocities quickly increase to their peaks after the ignition. The peak values are 0.030 m/s and 0.018m/s for the heptane and methanol fires, respectively. As the surface temperatures reach the boiling points, the convective motions tend to diminish. The maximum velocity attenuates to around 2 mm/s at 100 s. It can also be deduced that the convective motion is mainly caused by the Marangoni effect and the buoyancy effect plays less important role. This is also evidenced by the fact that the convective motion tends to diminish even if there still exist large temperature gradients inside the fuel region.

4.2 The transient thin-layer heptane pool fire

Comparison between the predicted and measured mass burning rate for the heptane fire is shown in Fig. 6. To investigate the effect of the convective motion on the burning rate, the predicted burning rate neglecting convection is also plotted. The simulation of no convection neglected the effects of both Marangoni and buoyancy, and only heat conduction was solved in the fuel region. The burning rate during the heat-up stage is well captured. Two distinct regimes in the early heat-up stage observed in the test was likely caused by the localized ignition source, which was not captured in current simulation as a constant initial burning rate across the fuel surface was used in the CFD simulation. From 50 s onwards, the measured burning rate remained almost constant, while the predicted value continues to increase gradually. This might have been caused by the increase in the container lip height due to the regression of the pool surface in the experiments, which would affect the magnitude of the mass burning rate as found by Dlugogorski and Wilson [24]. Moreover, the assumption of the adiabatic walls is also responsible for the over-prediction. The predicted burning rate without convection increases much quicker during the heat-up stage. Its value is much higher due to higher surface temperature, demonstrating that the convective motion significantly affects the mass burning rate, especially during the heat-up stage.

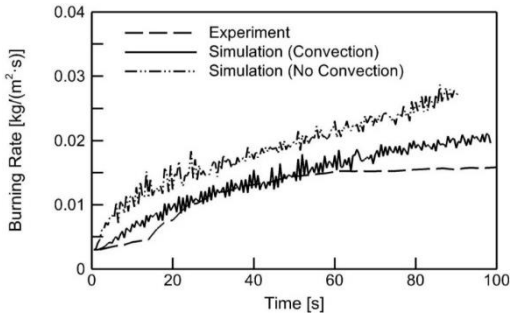

Fig. 6. Comparison between the predicted and measured [1] mass burning rate for the heptane fire.

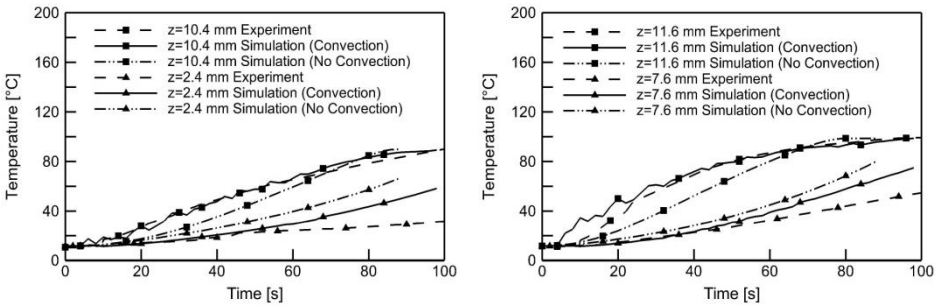

Fig. 7. Comparison between the predicted and measured [1] temperature profiles in the liquid at different locations for the heptane fire (z represents the vertical location from the fuel bottom).

The predicted temperature profiles in the liquid at four locations are compared with the measured profiles in Fig. 7 for the heptane case. The predicted profiles at the top two locations are in very good agreement with the measurements. The temperature profiles at the bottom two locations are over-predicted from approximately 50 s onwards. The assumption of the adiabatic bottom boundary condition is partly responsible for the over-predictions. The temperature profiles at the top two locations are apparently under-predicted by the simulation without convection, and over-predicted at the bottom two locations due to the over-prediction of the mass burning rate as mentioned above.

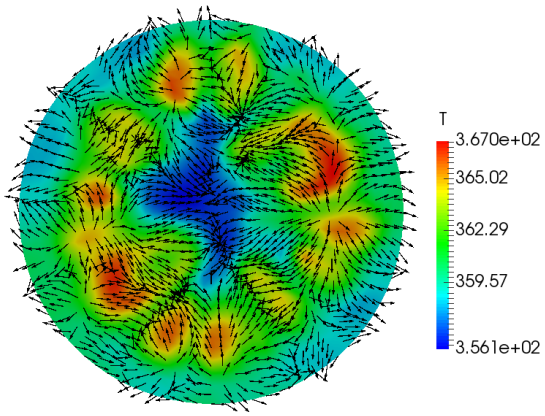

Fig. 8. The predicted temperature contour and velocity vectors at the pool surface at 30 s for the heptane fire.

Figure 8 shows the predicted temperature contour and velocity vector on pool surface at 30 s for the heptane fire, illustrating highly non-uniform distribution due to inhomogeneous heat feedback. It can also be observed that the surface Marangoni velocity is directed from the hot region to the cold region, tending to reduce the temperature gradient on the pool surface and promote more uniform distribution of the mass burning rate compared to the neglection of the convective motion.

5. Concluding remarks

A fully coupled 3-D numerical formulation has been formulated and validated. The fire dynamics was modelled using the in-house version of FireFOAM coupled with the simulation of the incompressible liquid fuel flow.

The predictions have been validated against measurements for both the gas and liquid phases achieving reasonably good agreement. It was found that the heat feedback to the pool surface are highly non-uniform, resulting in non-uniform distribution of the mass burning rate and inducing the convective motion in the liquid pool. Counter-rotating vortices were well captured and found to apparently enhance heat transfer within the liquid fuel. It was also observed that the convective motion gradually attenuated once the liquid region was heated up to a more uniform temperature distribution and the convective motion was mainly caused by the Marangoni effect. Finally, the convective motion in the liquid phase was found to play an important role in the predictions of the mass burning rate. Neglecting the convective motion would result in faster rise and over-prediction of the mass burning rate. It was also found that the convective motion is mainly caused by the Marangoni effect and the buoyancy effect has much less influence.

Acknowledgement

The authors are grateful to EPSRC (grant number: EP/R029369/1) and ARCHER for financial and computational support as a part of their funding to the UK Consortium on Turbulent Reacting Flows (www.ukctrf.com). Funding is also acknowledged to University of Warwick through granting Jennifer Wen a discretionary budget which financed Baopeng Xu's part time effort.

References

[1] Q. Kang, S. Lu, B. Chen, Experimental study on burning rate of small scale heptane pool fires. Chin. Sci. Bull, 10 (2010) 81-87.

[2] J. Zhao, H. Huang, G. Jomaas, M. Zhong, R. Yang, Experimental study of the burning behaviors of thin-layer pool fires, Combust. Flame 193 (2018) 327-334.

[3] J. Garo, J. Vantelon, H. Koseki, Thin-layer boilover: prediction of its onset and intensity, Combust. Sci. Technol. 178 (2006) 1217–1235.

[4] J. Garo, P. Gillard, J. Vantelon, A. Fernandez, Combustion of Liquid Fuels Spilled on Water. Prediction of Time to Start of Boilover, Combust. Sci. Technol. 147 (1-6) (1999) 39-59.

[5] H. Koseki, G. W. Mulholland, The effect of diameter on the burning of crude oil pool fires, Fire Technol. 27 (1) (1991) 54-65.

[6] A. Hamins, M. Klassen, J. Gore, S. Fischer, T. Kashiwagi, Heat feedback to the fuel surface in pool fires, Combust. Sci. Technol. 97 (1-3) (1994) 37-62.

[7] A. Hamins, A. Lock, The Structure of a Moderate-Scale Methanol Pool Fire. Report No. NIST-1928, National Institute of Standards and Technology, 2016.

[8] E.J. Weckman, A.B. Strong, Experimental investigation of the turbulence structure of medium-scale methanol pool fires, Combust. Flame 105 (3) (1996) 245-266.

[9] H. Hayasaka, Unsteady burning rates of small pool fires, Fifth International Symposium on Fire Safety Science, Australia, 1997, p. 499.

[10] V. Babrauskas, Estimating large pool fire burning rates, Fire Technol. 19 (4) (1983) 251-261.

[11] K. Akita, T. Yumoto, Heat transfer in small pools and rates of burning of liquid methanol. Proc. Combust. Inst. 10 (1) (1965) 943-948.

[12] H. Farahani, G. Jomaas, A. Rangwala, Effects of convective motion in n-octane pool fires in an ice cavity, Combust. Flame 162 (12) (2015) 4643-4648.

[13] V.I. Blinov, G.N. Khudiakov, The burning of liquid pools, Doklady Akademi Nauk SSSR, 113 (1957) 1094-1098.

[14] K. Akita, T. Yumoto, Heat transfer in small pools and rates of burning of liquid methanol, Proc. Combust. Inst. 10 (1) (1965) 943-948.

[15] D. Villers, J.K. Platten, Coupled buoyancy and Marangoni convection in acetone: experiments and comparison with numerical simulations, J. Fluid Mech. 234 (1992) 487–510.

[16] Z.B. Chen, J. Wen, B.P. Xu, S. Dembele, Large eddy simulation of a medium-scale methanol pool fire using the extended eddy dissipation concept, Int. J. Heat Mass Tran. 70 (2014) 389-408.

[17] M.L. Janssens, S.E. Dillon, S. Allwein, Burning Characteristics of Heptane and Methanol Pool Fires, Seventh International Conference on Fire and Materials, USA, 2001, p. 517.

[18] T. Sikanen, S. Hostikka, Modelling and simulation of liquid pool fires with in-depth radiation and heat transfer, Fire Saf. J. 80 (2016) 95–109.

[19] T. Beji, B. Merci, Development of a numerical model for liquid pool evaporation, Fire Saf. J. 102 (2018) 48–58.

[20] K. Fukumoto, J. Wen, M. Li, Y. Ding, C. Wang, Numerical simulation of small pool fires incorporating liquid fuel motion, Combust. Flame 213 (2020) 441-454.

[21] Y. Wang, K. Meredith, P. Chatterjee, N. Krishnamoorthy, X. Zhou, S. Dorofeev, Status of FireFOAM development and future plan, in: 3rd FM Glob. Open Source CFD Fire Model. Work. Norwood, MA, USA, 2011.

[22] S. Menson, P.K. Yeung, W.W. Kim, Effect of subgrid models on the computed interscale energy transfer in isotropic turbulence, Comput. Fluids 25 (2) (1996) 165-180.

[23] J. Staggs, The effects of gas-phase and in-depth radiation absorption on ignition and steady burning rate of PMMA, Combust. Flame 161 (12) (2014) 3229–3236.

[24] B.Z. Dlugogorcki, M. Wilson, Effect of lip height on properties of small scale pool fires, Fire Saf. Sci. 2 (1995) 129-140.

[25] A. Vali, D.S. Nobes, L.W. Kostiuk, Transport phenomena within the liquid phase of a laboratory-scale circular methanol pool fire, Combust. Flame 161 (2014) 1076–1084.

[26] J. Zhao, H. Huang, H. Wang, J. Zhao, Q. Liu, Y. Li, Experimental study on burning behaviors and thermal radiative penetration of thin-layer burning, J. Therm. Anal. Calorim. 130 (2017) 1153-62.

[27] T. Sikanen , S. Hostikka , Modeling and simulation of liquid pool fires with in- depth radiation absorption and heat transfer, Fire Safety J. 80 (2016) 95–109 .

List of Figure Captions

Fig. 1. Comparison between the predicted flame shapes (bottom) with the images from the methanol fire test [7].

Fig. 2. The time-averaged incident radiative heat and convective fluxes at the pool surface for the methanol fire.

Fig. 3. Comparison between the predicted and measured gas phase time-averaged temperatures and species concentrations for the methanol fire.

Fig. 4. The predicted mass burning rate vs time and the comparison between the predicted and measured [7] time-averaged distribution at the pool surface.

Fig. 5. The predicted velocity vectors at the middle plane for the methanol fire and the maximum velocity in the fuel region.

Fig. 6. Comparison between the predicted and measured [1] mass burning rate for the heptane fire.

Fig. 7. Comparison between the predicted and measured [1] temperature profiles in the liquid at different locations for the heptane fire. (z represents the vertical location from the fuel bottom.)

Fig. 8. The predicted temperature contour and velocity vectors at the pool surface at 30 s for the heptane fire.